CDF Note 9217

Search for Electroweak Single Top-Quark Production using Neural Networks with 2.2 fb^{-1} of CDF II data

The CDF Collaboration
URL http://www-cdf.fnal.gov
(Dated: March 12, 2008)

We report on a search for electroweak single top–quark production with CDF II data corresponding to 2.2 fb^{-1} of integrated luminosity. We apply neural networks to construct discriminants that distinguish between single top–quark and background events. We combine t- and s-channel events to one single top–quark signal assuming the ratio of the two processes is given by the standard model (SM) and assuming a top quark mass of 175 GeV/c^2. Using ensemble tests, we determine that we expect with a probability of 50% to see a single top signal that is larger than a 4.4σ fluctuation of the background (p–value of 0.0000053). A binned likelihood fit to data yields a cross section of $2.0^{+0.9}_{-0.8}$ pb for single top–quark production. The observed p–value is 0.00063 which corresponds to a significance of 3.2σ.

Preliminary Results for Winter 2008 Conferences

I. INTRODUCTION

According to the standard model, in $p\bar{p}$ collisions at the Tevatron top quarks can be created in pairs via the strong force, of singly via the electroweak interaction. The latter production mode is referred to as "single top–quark" production and takes place mainly through the s- or t- channel exchange of a W boson. The CDF and DØ collaborations have published single top–quark results at $\sqrt{s} = 1.8$ TeV and $\sqrt{s} = 1.96$ TeV [1–3]. The most recent result from the DØ collaboration [3] has seen evidence for single top quark production and measured $\sigma_{\text{single top}} = 4.9 \pm 1.4$ pb.
The theoretical single top–quark production cross section is $\sigma_{\text{single top}} = 2.9 \pm 0.4$ pb for a top–quark mass of 175 GeV/c^2 [4]. Despite this small rate, the main obstacle in finding single top–quarks is in fact the large associated background. After all section requirements are imposed, the signal to background ratio is approximately 1/20. This challenging, background-dominated dataset is the main motivation for using multivariate techniques.

II. COMMON EVENT SELECTION

The CDF event selection exploits the kinematic features of the signal final state, which contains a top quark, a bottom quark, and possibly additional light quark jets. To reduce multijet backgrounds, the W originating from the top quark is required to have decayed leptonically. One therefore demands a single high-energy electron or muon ($E_T(e) > 20$ GeV, or $P_T(\mu) > 20$ GeV/c) and large missing transverse energy $\not\!\!E_T > 25$ GeV from the undetected neutrino.
The backgrounds belong to the following categories: $Wb\bar{b}$, $Wc\bar{c}$, Wc, mistags (light quarks misidentified as heavy flavor jets), top pair production $t\bar{t}$ events (one lepton or two jets are lost due to detector acceptance), non-W (QCD multijet events where a jet is erroneously identified as a lepton), $Z \to ll$ and diboson WW, WZ, and ZZ. We remove a large fraction of the backgrounds by demanding two or three jets with $E_T > 20$ GeV and $|\eta| < 2.8$ be present in the event. At least one of these jets has to be tagged as a b quark jet by using displaced vertex information from the silicon vertex detector (SVX) of CDF [5]. The non-W content of the selected electron dataset is further reduced by several requirements to transverse mass of the W-boson candidate, the missing transverse energy significance, the angle between the $\not\!\!E_T$ vector and the transverse momentum vector and the angle between the charged lepton and the momentum vector of the jets. The numbers of expected and observed events are listed in table I.

Process	Number of Events			
	2–jet–bin		3–jet–bin	
	1–tag–bin	2–tag–bin	1–tag–bin	2–tag–bin
$t\bar{t}$	94.8 ± 13.3	21.1 ± 3.5	204.1 ± 28.5	60.3 ± 9.9
$Wb\bar{b}$	376.2 ± 113.4	49.7 ± 15.5	106.7 ± 32.2	17.6 ± 5.5
$Wc\bar{c}/Wc$	361.4 ± 111.4	4.8 ± 1.6	92.7 ± 28.5	2.4 ± 0.8
Mistags	308.3 ± 51.1	1.2 ± 0.4	88.6 ± 14.8	0.9 ± 0.3
Non–W	55.8 ± 22.3	1.5 ± 0.6	21.3 ± 8.5	0.2 ± 0.1
Diboson	52.4 ± 5.2	3.2 ± 0.3	16.7 ± 1.7	1.1 ± 0.1
Z+jets	19.1 ± 2.8	0.9 ± 0.1	7.1 ± 1.0	0.5 ± 0.1
t–channel	50.6 ± 7.4	1.4 ± 0.2	13.1 ± 1.9	2.1 ± 0.3
s–channel	26.3 ± 3.7	7.6 ± 1.2	8.2 ± 1.2	2.7 ± 0.4
total background	1268.0 ± 319.5	82.4 ± 22.0	537.2 ± 115.2	83.0 ± 16.8
total single–top	76.9 ± 11.1	9.0 ± 1.4	21.3 ± 3.1	4.8 ± 0.7
total prediction	1345.0 ± 231.9	91.3 ± 17.6	558.7 ± 68.8	87.8 ± 11.6
observation	1312	82	491	95

TABLE I: Expected number of signal and background events and total number of events observed in 2.2 fb^{-1} in the CDF single top–quark dataset.

III. NEURAL NETWORK INPUT VARIABLES

Using neural networks many kinematic or event shape variables are combined to a powerful discriminant. In the search for single top–quark production, four different neural networks are trained in different jet and tag bins:

- 2 jets, 1 tag: t–channel
- 2 jets, 2 tags: s–channel
- 3 jets, 1 tag: t–channel
- 3 jets, 2 tags: t–channel

The 2jets, 1tag sample is the largest sub sample and dominates so the search for single top–quarks. The four most important variables of the the NN in the 2 jets, 1tag sample are the reconstructed top quark mass, the KIT flavor separator, the invariant mass of the two jets and the product of the lepton-charge and the pseudorapidity of the light quark, see figure 1. For each variable the signal and background shapes, a data Monte-Carlo comparison and a check of the background shape in the zero-tag sample are shown in figure 1. The KIT flavor separator gives an additional handle to reduce the large background components where no real b quarks are contained, mistags and charm-backgrounds. Both of them amount to about 50% in the W+2 jets data sample even after imposing the requirement that one jet is identified by the secondary vertex tagger of CDF [5].

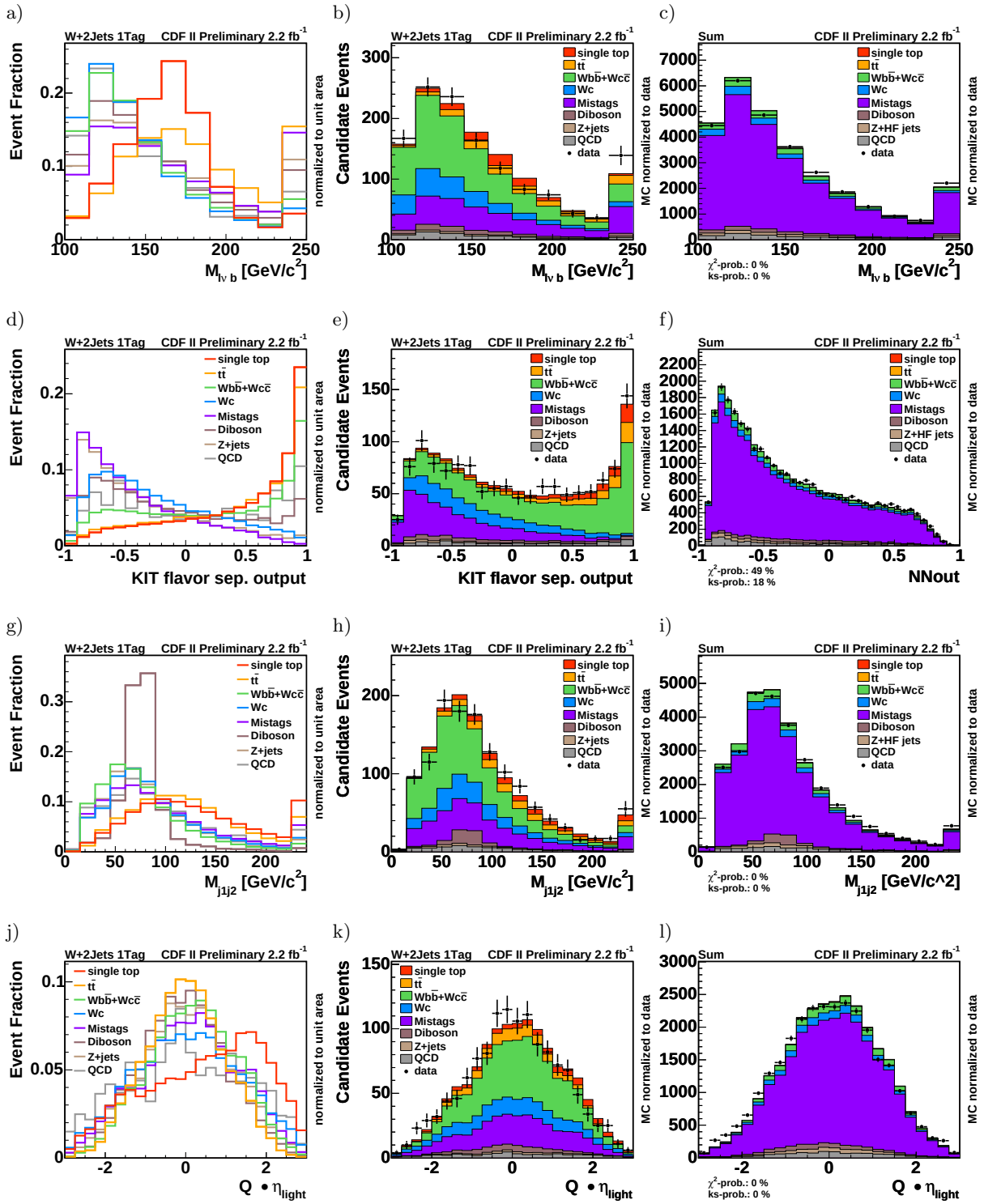

FIG. 1: *Some of the most powerful variables in the 2jet, 1tag sample. Left: signal and background shapes, Middle: Data-Monte Carlo comparison, Right: Check of background shapes in the W+2jet zero tag sample.*

IV. TEMPLATES FOR BINNED LIKELIHOOD FIT

The training of a neural network results in one output variable continuously distributed between -1 and 1. The output of the different neural networks is used to create signal and background templates which are to be fitted to the output distribution of observed events. We perform a combined single top–quark search meaning that the output distributions of both t– and s–channel events are combined into one single distribution, where the ratio between the two processes is as predicted by the standard model. In the fit, all considered sub sample (2 jets 1tag, 2 jets 2tags, 3 jet 1 tag and 3jet 2 tags) are fitted simultaneously to determine the combined single top–quark cross section.

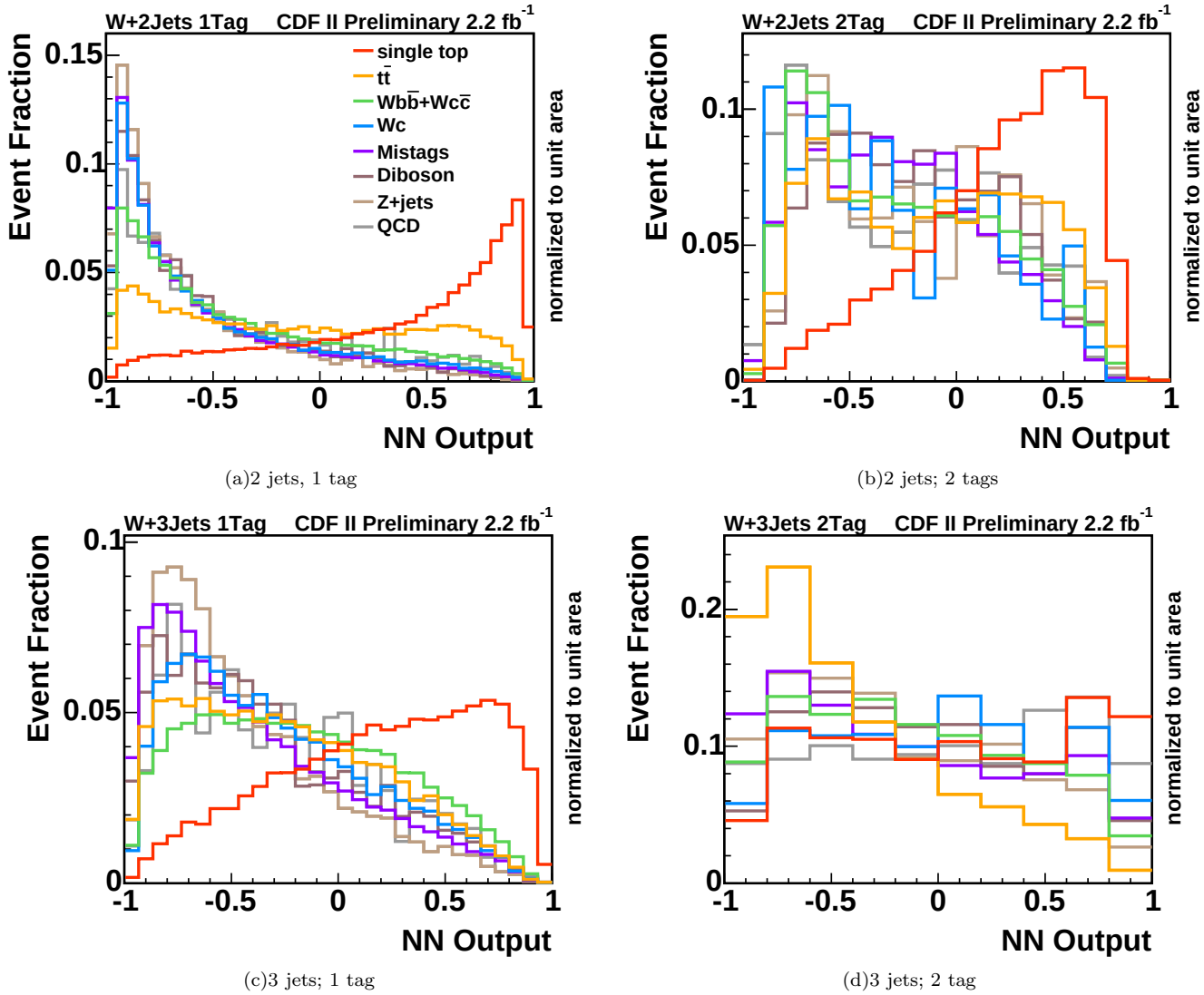

(a)2 jets, 1 tag

(b)2 jets; 2 tags

(c)3 jets; 1 tag

(d)3 jets; 2 tag

FIG. 2: The templates for the combined search are built using the following networks: the (a) t–channel neural network in the 2–jet bin with 1 b–tag, (b) s–channel neural network in the 2–jet bin with 2 b–tags, and the (c) t–channel neural network in the 3–jet bin with 1 b–tag and with 2 b–tags (d). The output of t– and s–channel events is added with a ratio corresponding to the standard–model prediction.

Figure 2 shows the templates of the combined single top–quark search. The t–channel templates in the 2–jet bin with 1 b–tag and in the 3–jet bin with 1 and 2 b–tags are presented in figure 2(a), 2(c) and 2(d), while the s–channel templates in the 2–jet bin with 2 b–tags are presented in figure 2(b).

V. SYSTEMATIC UNCERTAINTIES

Systematic uncertainties can cause a shift in the event detection efficiency for events of different physics processes, but can also cause a change in the shape of the template distributions.
The rate uncertainties are summarized in tables II-V separately for the four sub samples. They are only determined for single top–quark and $t\bar{t}$ events because the rates of the main backgrounds, W+jets and non–W events, are estimated based on the observed rate of events before b tagging or by a fit to the observed missing transverse energy distribution, respectively.
The following sources of systematic shape uncertainties are considered: the jet energy scale (JES), initial state gluon radiation (ISR), final state gluon radiation (FSR), parton distribution functions (PDFs), KIT flavor separator, the factorization and renormalization scale for W + heavy flavor processes, the reweighting of the mismodeld variables ΔR_{j1j2} and η_{j2}, the modeling of mistag events, the flavor composition and modeling of non-W events.
The shape uncertainties are determined by altering the respective effects within their uncertainties. In this way two shifted distributions are obtained for first five sources (see first two examples in figure 3), one plus and one minus distribution. For the last five systematic sources one alternative model is considered. Therefore, only one systematic shape is obtained for theses effects (see third example in figure 3).

Source	t-channel	s-channel	single top	$t\bar{t}$
ISR less/more	2.8/-0.2 %	0.3/6.7 %	1.9/2.1 %	-2.6/-7.1 %
FSR less/more	4.2/-1.3 %	5.9/0.4 %	4.8/-0.7 %	-5.1/-2.6 %
PDF	3.4/-3.4 %	2.2/-2.2 %	3.0/-3.0 %	1.8/-1.8 %
MC	2.0/-2.0 %	1.0/-1.0 %	1.7/-1.7 %	-2.7/2.7 %
$\epsilon_{\rm evt}$	4.2/-4.2 %	2.3/-2.3 %	3.6/-3.6 %	2.9/-2.9 %
Luminosity	6.0/-6.0 %	6.0/-6.0 %	6.0/-6.0 %	6.0/-6.0 %
Cross section	12.6/-12.6 %	12.4/-12.4 %	12.6/-12.6 %	12.4/-12.4 %
$M_{\rm top}$ 170/180	1.3/-0.8 %	2.4/-1.7 %	1.7/-1.1 %	-3.1/1.4 %
	Diboson	Z+jets		
$\epsilon_{\rm evt}$	7.6/-7.6 %	8.3/-8.3 %		
Luminosity	6.0/-6.0 %	6.0/-6.0 %		
Cross section	1.9/-1.9 %	10.8/-10.8 %		

TABLE II: Systematic rate uncertainties for 2 jets and 1 b tag

Source	t-channel	s-channel	single top	$t\bar{t}$
ISR less/more	-4.9/-6.9 %	1.3/9.2 %	0.4/6.7 %	0.5/-9.5 %
FSR less/more	3.9/-6.6 %	8.1/2.2 %	7.5/0.8 %	-8.1/-1.8 %
PDF	2.0/-2.0 %	2.0/-2.0 %	2.0/-2.0 %	1.7/-1.7 %
MC	2.0/-2.0 %	1.0/-1.0 %	1.2/-1.2 %	4.6/-4.6 %
$\epsilon_{\rm evt}$	10.0/-10.0 %	8.7/-8.7 %	8.9/-8.9 %	9.0/-9.0 %
Luminosity	6.0/-6.0 %	6.0/-6.0 %	6.0/-6.0 %	6.0/-6.0 %
Cross section	12.6/-12.6 %	12.4/-12.4 %	12.5/-12.5 %	12.4/-12.4 %
$M_{\rm top}$ 170/180	-4.7/-4.1 %	2.1/0.1 %	1.0/-0.5 %	0.4/3.0 %
	Diboson	Z+jets	Mistags	
$\epsilon_{\rm evt}$	9.8/-9.8 %	10.6/-10.6 %		
Luminosity	6.0/-6.0 %	6.0/-6.0 %		
Double tag			23.4/-23.4%	
Cross section	1.9/-1.9 %	10.8/-10.8 %		

TABLE III: Systematic rate uncertainties for 2 jets and 2 b tags

Source	t-channel	s-channel	single top	$t\bar{t}$
ISR less/more	-6.8/-0.0 %	2.4/-12.6 %	-3.3/-4.8 %	-0.6/-4.6 %
FSR less/more	-1.5/-3.1 %	-6.0/-4.8 %	-3.3/-3.8 %	-3.5/-2.2 %
PDF	2.7/-2.7 %	2.3/-2.3 %	2.6/-2.6 %	1.8/-1.8 %
MC	1.9/-1.9 %	1.5/-1.5 %	1.7/-1.7 %	-1.7/1.7 %
$\epsilon_{\rm evt}$	3.5/-3.5 %	2.3/-2.3 %	3.0/-3.0 %	2.3/-2.3 %
Luminosity	6.0/-6.0 %	6.0/-6.0 %	6.0/-6.0 %	6.0/-6.0 %
Cross section	12.6/-12.6 %	12.4/-12.4 %	12.6/-12.6 %	12.4/-12.4 %
$M_{\rm top}$ 170/180	1.5/-2.8 %	6.0/-2.7 %	3.2/-2.7 %	-0.7/0.8 %
	Diboson	Z+jets		
$\epsilon_{\rm evt}$	7.8/-7.8 %	7.8/-7.8 %		
Luminosity	6.0/-6.0 %	6.0/-6.0 %		
Cross section	1.9/-1.9 %	10.8/-10.8 %		

TABLE IV: Systematic rate uncertainties for 3 jets and 1 b tag

Source	t-channel	s-channel	single top	$t\bar{t}$
ISR less/more	7.8/3.2 %	4.3/-11.2 %	5.8/-4.9 %	-0.5/-6.6 %
FSR less/more	15.0/1.3 %	-7.4/-5.0 %	2.4/-2.2 %	-3.4/-2.7 %
PDF	1.5/-1.5 %	2.1/-2.1 %	1.9/-1.9 %	1.7/-1.7 %
MC	1.9/-1.9 %	1.5/-1.5 %	1.7/-1.7 %	2.0/-2.0 %
$\epsilon_{\rm evt}$	9.1/-9.1 %	8.8/-8.8 %	8.9/-8.9 %	9.1/-9.1 %
Luminosity	6.0/-6.0 %	6.0/-6.0 %	6.0/-6.0 %	6.0/-6.0 %
Cross section	12.6/-12.6 %	12.4/-12.4 %	12.5/-12.5 %	12.4/-12.4 %
$M_{\rm top}$ 170/180	4.2/3.0 %	1.6/-6.8 %	2.7/-2.5 %	-0.6/-1.0 %
	Diboson	Z+jets	Mistags	
$\epsilon_{\rm evt}$	10.8/-10.8%	11.1/-11.1 %		
Luminosity	6.0/-6.0 %	6.0/-6.0 %		
Double tag			23.4/-23.4%	
Cross section	1.9/-1.9 %	10.8/-10.8 %		

TABLE V: Systematic rate uncertainties for 3 jets and 2 b tags

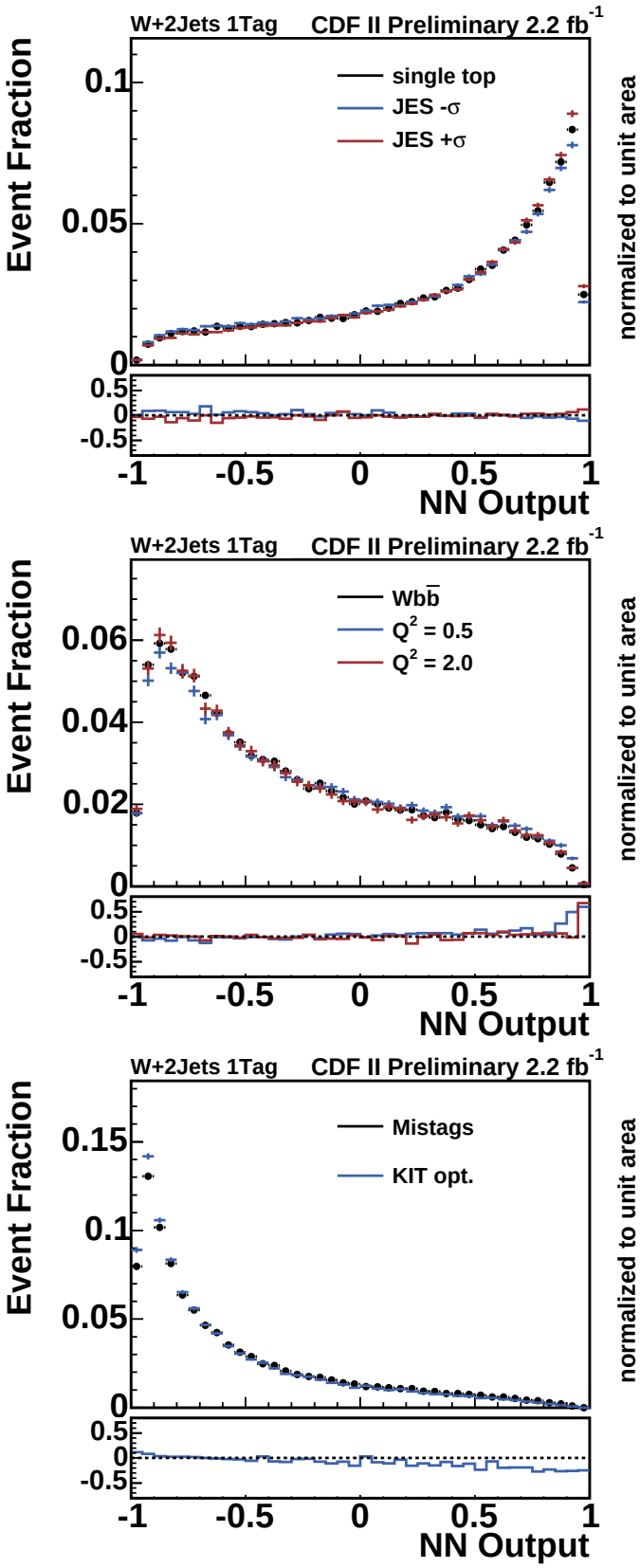

FIG. 3: Examples of shape uncertainties. Shown is the comparison between the default distribution and the shifted distribution. Top: Shape systematics due the uncertainty on the jet energy correction for single top–quark production. Center: Shape systematics due the uncertainty on the renormalization scale Q^2 for $Wb\bar{b}$. Bottom: Shape systematics due to the uncertainty on the output of the KIT flavor separator for mistag events.

VI. LIKELIHOOD FUNCTION

The likelihood function consists of Poisson terms for the individual bins of the fitted histograms, Gaussian constraints to the background rates, and Gaussian constraints to the strengths of systematic effects.

$$L(\beta_1, \dots, \beta_5; \delta_1, \dots, \delta_S) = \prod_{k=1}^{B} \frac{e^{-\mu_k} \cdot \mu_k^{n_k}}{n_k!} \cdot \prod_{j=2}^{5} G(\beta_j, 1.0, \Delta_j) \cdot \prod_{i=1}^{S} G(\delta_i, 0.0, 1.0); \tag{1}$$

Systematic uncertainties are included as factors modifying the expectation value μ_k of events in a certain bin k.

$$\mu_k = \sum_{j=1}^{5} \beta_j \cdot \nu_j \cdot \mathcal{L}_{\text{int}} \cdot \left\{ \prod_{i=1}^{S} (1 + \delta_i \cdot \epsilon_{ji}) \right\} \cdot \alpha_{jk} \cdot \left\{ 1 + \sum_{i=1}^{S} (\delta_i \cdot \kappa_{jik}) \right\} \tag{2}$$

The index j runs over the different physics processes that occur in the likelihood function. The cross section of process j is σ_j. In the likelihood function we use the parameter β_j, which is the cross section normalized to its standard model prediction. The event detection efficiency of process j is named ν_j. The normalized content of bin k of the template histogram for process j is α_{jk}.
Rate uncertainties as well as uncertainties in shape are considered. The sources of systematic uncertainties are indexed with i. The relative acceptance uncertainties due to these sources are named ϵ_{ji}. The relative uncertainties in the bin content of bin k of the template histograms are called κ_{jik}. The variation in strength of a systematic effect i is measured with the variable δ_i.
The shape uncertainties are calculated from the systematically shifted histograms α^+_{jik} and α^-_{jik} according to

$$\kappa_{jik} = \frac{\alpha^+_{jik} - \alpha^-_{jik}}{2\,\alpha_{jk}} \tag{3}$$

By construction the κ_{jik} satisfy the normalization condition

$$\sum_{k=1}^{B} \kappa_{jik} = 0\ . \tag{4}$$

The systematically shifted template that takes into account the shifts caused by all systematic effects with strengths $\{\delta_i\}$ is given by

$$\alpha'_{ji} = \alpha_{jk} \cdot \left\{ 1 + \sum_{i=1}^{S} \delta_i \cdot \kappa_{jik} \right\} \tag{5}$$

Due to (4) the shifted histogram α'_{ji} is properly normalized:

$$\sum_{k=1}^{B} \alpha'_{ji} = 1\ . \tag{6}$$

The background rates (cross sections) and the parameters describing the strength of systematic excursions (δ_i) are constrained by additional Gaussian terms in the likelihood. The background rates are constraint within the uncertainties of the prediction, Δ_j. The strengths of the systematic effects are constraint to 0.0 with a standard deviation of 1.0. The single top–quark content (cross section) is measured by fitting the parameters (β_j and δ_j) of the likelihood function to the observed data. This is achieved by minimizing the log likelihood with respect to these parameters using the program MINUIT.

Using this technique one can compute the likelihood as a function of the single top–quark production cross section, β_1, only. The log likelihood is minimized at a fixed value of β_1 with respect to all other variables which are also often called *nuisance* parameters. The resulting one-dimensional function is called the reduced likelihood, $\mathcal{L}_{\text{red}}(\beta_1)$. This method is often called *profiling* the likelihood function.

VII. EXPECTED SENSITIVITY AND SIGNIFICANCE

We use ensemble tests to compute the sensitivity of our analysis. An ensemble test consists of a set of pseudo experiments. For each pseudo experiment we determine first the number of events N_j of each process by drawing a random number from a Poisson distribution with a mean μ_j. In a second step we draw random numbers from the template distributions of the neural network output.

To compute the significance of a potentially observed signal, we perform a hypothesis test. Two hypotheses are considered. The first one, H_0, assumes that the single top–quark cross section is zero ($\beta_1 = 0$) and is called the *null hypothesis*. The second hypothesis, H_1, assumes that the single top–quark production cross section is the one predicted by the standard model ($\beta_1 = 1$). The objective of our analysis is to observe single top–quarks, that means to reject the null hypothesis H_0.

The hypothesis test is based on the Q-value,

$$Q = -2\left(\ln L_{\rm red}(\beta_1 = 1) - \ln L_{\rm red}(\beta_1 = 0)\right) , \tag{7}$$

where $L_{\rm red}(\beta_1 = 1)$ is the value of the reduced likelihood function at the standard model prediction and $L_{\rm red}(\beta_1 = 0)$ is the value of the reduced likelihood function for a single top–quark cross section of zero. Using the two ensemble tests the distribution of Q-values is determined for the case with single top–quarks included at the standard model rate, q_1, and for the case of zero single top–quark cross section, q_0. The two Q-value distributions are shown in figure 4.

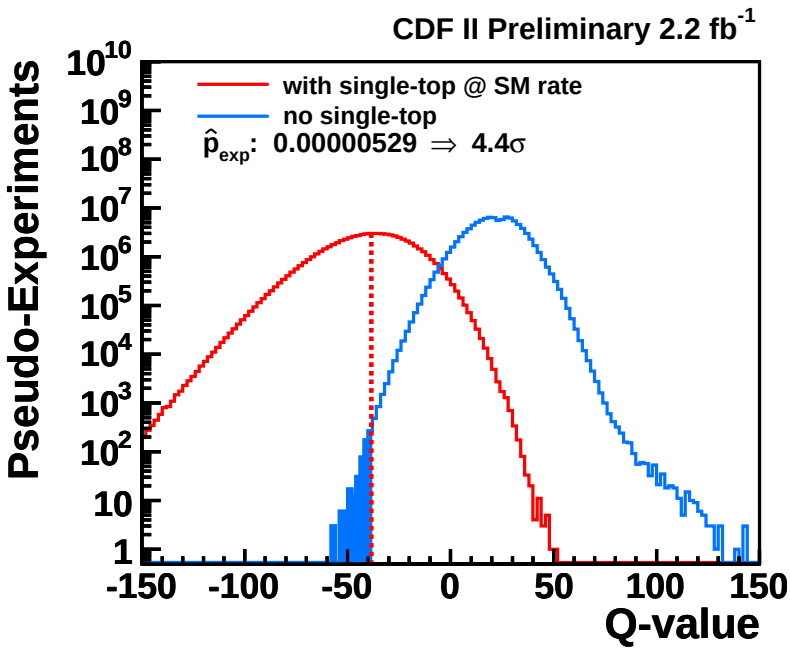

FIG. 4: Distributions of Q-values for two ensemble tests, one with single top–quark events present at the expected standard model rate, one without any single top–quark events.

To quantify the sensitivity of our analysis we define the expected p-value $\hat{p} = p(Q_1^{\rm med})$ where $Q_1^{\rm med}$ is the median of the Q-value distribution q_1 for the hypothesis H_1. The meaning of $\hat{p}$ is the following: Under the assumption that H_1 is correct one expects to observe $p < \hat{p}$ with a probability of 50%. We find $\hat{p} = 0.0000053$, including all systematic uncertainties. In other words, assuming the predicted single top–quark production cross–section, we expect with a probability of 50% , to see at least that many single top–quark events that the observed excess over the background corresponds to a background fluctuation of 4.4σ in case of the combined search.

VIII. BINNED LIKELIHOOD FIT TO DATA

The neural networks are applied to the observed events. The predicted and measured output distribution of all four neural networks used in the combined search are depicted in figure 5. In figure 6 the distributions of all four neural networks are added together.

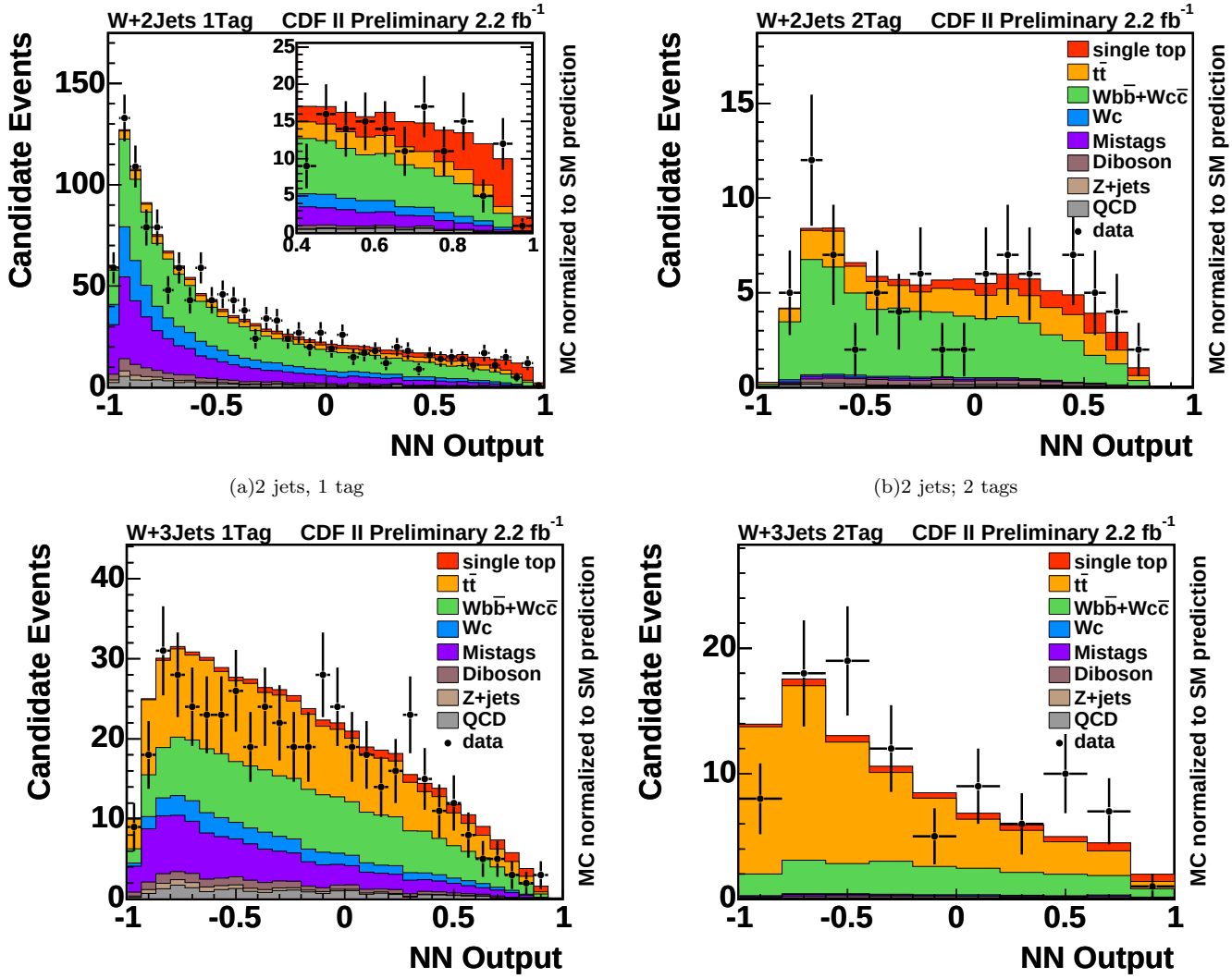

(a)2 jets, 1 tag

(b)2 jets; 2 tags

(c)3 jets; 1 tag

(d)3 jets; 2 tag

FIG. 5: Distributions of observed data and MC normalized to the prediction for the following networks: the (a) t–channel neural network in the 2–jet bin with 1 b–tag, (b) s–channel neural network in the 2–jet bin with 2 b–tags, and the (c) t–channel neural network in the 3–jet bin with 1 b–tag and with 2 b–tags (d). The output of t– and s–channel events is added with a ratio corresponding to the standard–model prediction.

Finally, the templates are fitted to the observed distributions to determine the single top–quark cross section. The fit yields a single top–quark cross section of $2.0^{+0.9}_{-0.8}$pb. As depicted in figure 7, the fitted distributions describe the observed output distributions of the four sub samples well. In figure 8 the distributions of all four neural networks are added together.

Figure 9, compares the observed Q–value with the expectation. The observed p–value is 0.00063 corresponding to a significance of 3.2σ.

The distribution of the reconstructed to mass, the output of the KIT flavor separator, as well as the product of the lepton-charge and the pseudo-rapidity of the light-quark jet are presented in figure 10 for the high NN output regions $NN > 0.4$ and $NN > 0.8$.

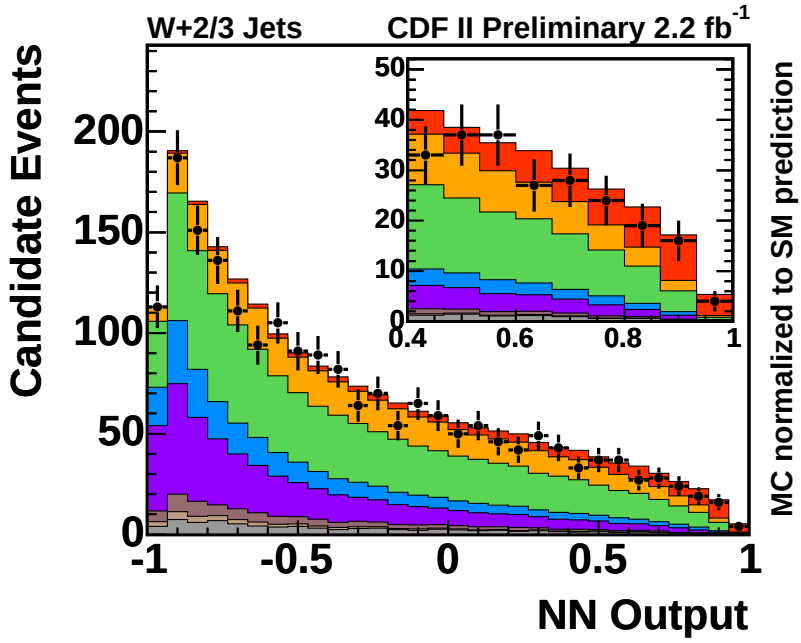

FIG. 6: Distributions of observed data and MC normalized to the prediction for all four networks. The output of t– and s–channel events is added with a ratio corresponding to the standard–model prediction.

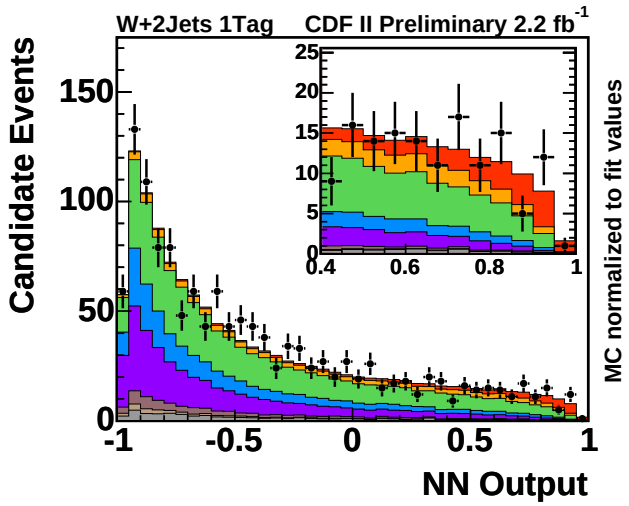

(a)2 jets, 1 tag

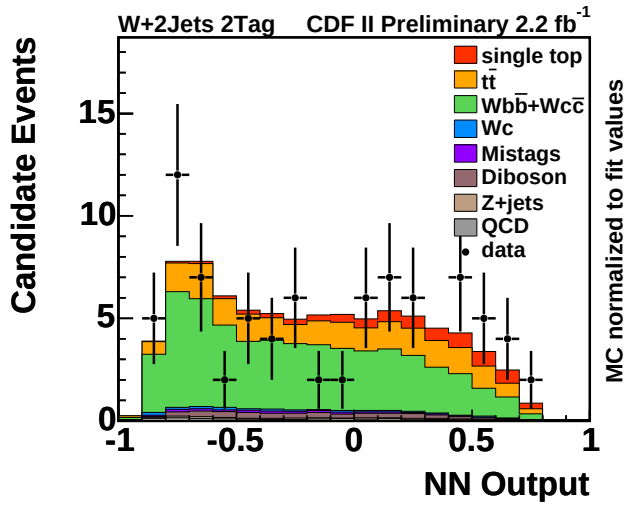

(b)2 jets; 2 tags

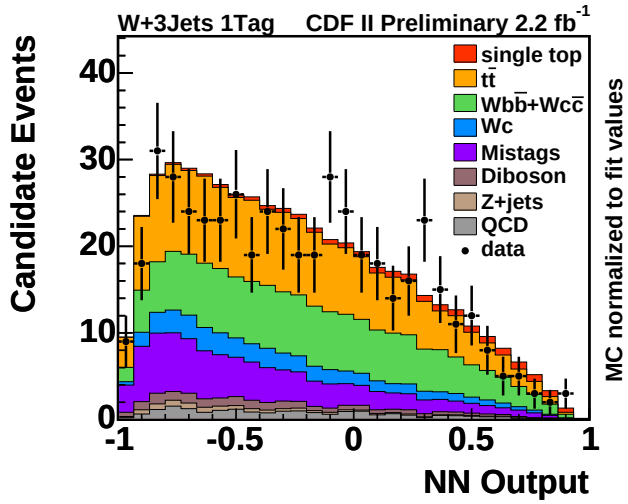

(c)3 jets; 1 tag

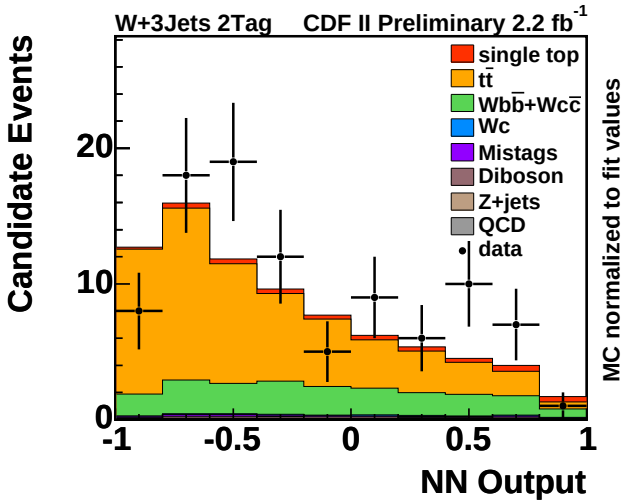

(d)3 jets; 2 tag

FIG. 7: Distributions of observed data and MC normalized to the simultaneously fitted values for the following networks: the (a) t–channel neural network in the 2–jet bin with 1 b–tag, (b) s–channel neural network in the 2–jet bin with 2 b–tags, and the (c) t–channel neural network in the 3–jet bin with 1 b–tag and with 2 b–tags (d). The output of t– and s–channel events is added with a ratio corresponding to the standard–model prediction.

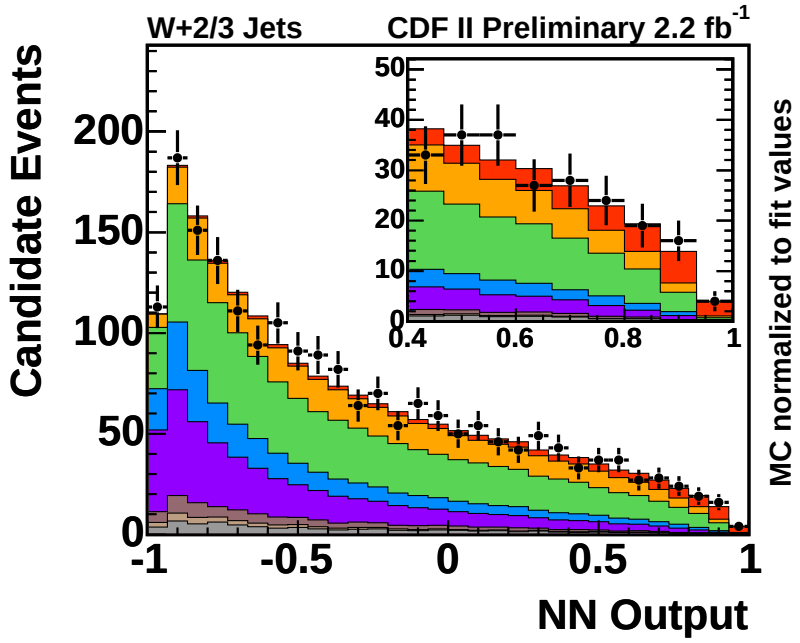

FIG. 8: Distributions of observed data and MC normalized to the simultaneously fitted values for all four networks. The output of t– and s–channel events is added with a ratio corresponding to the standard–model prediction.

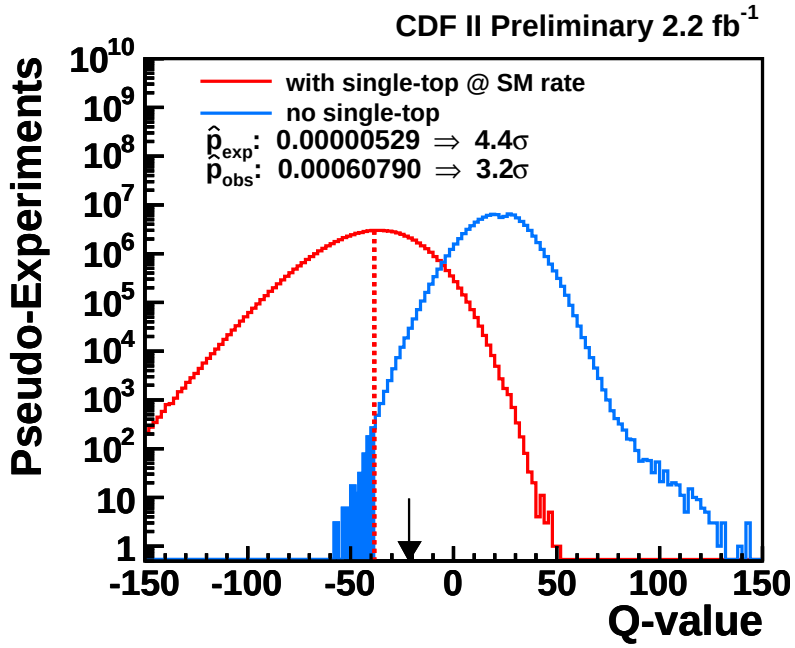

FIG. 9: Comparison of observed Q–value to the expectation in the combined search.

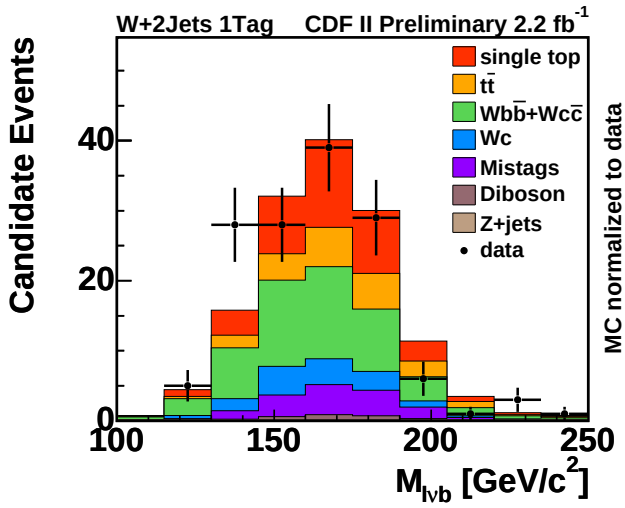

(a)M_{lnub}, $NN > 0.4$

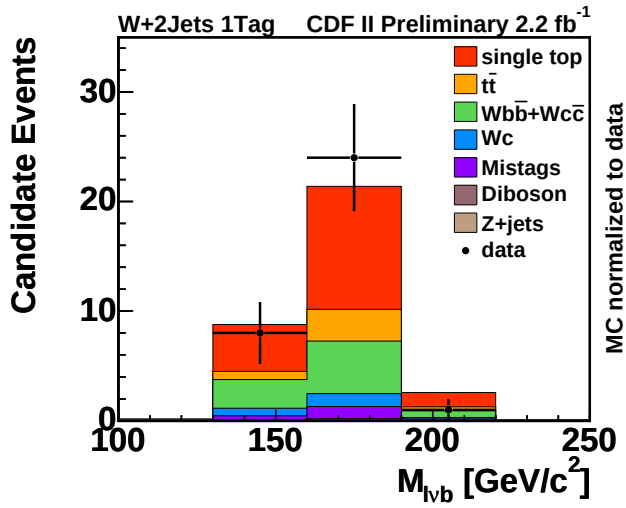

(b)M_{lnub}, $NN > 0.8$

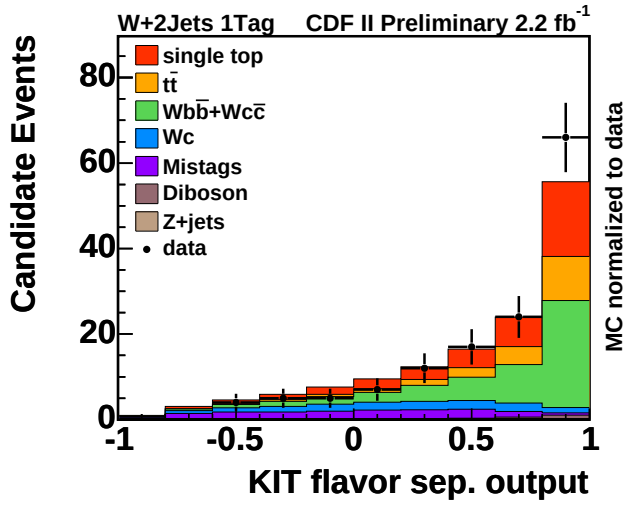

(c)KIT flavor separator, $NN > 0.4$

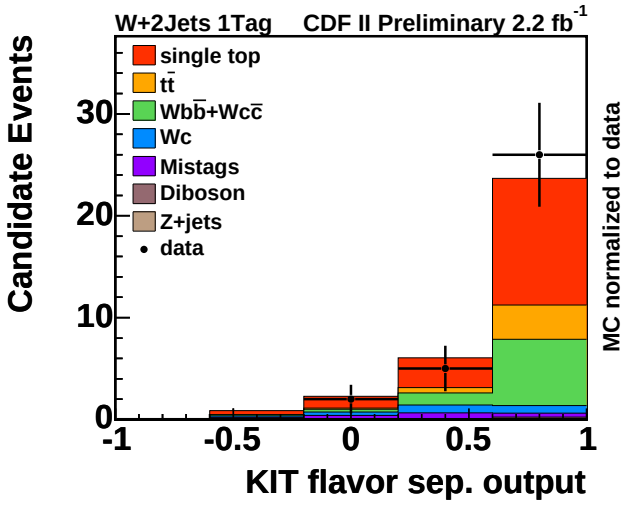

(d)KIT flavor separator, $NN > 0.8$

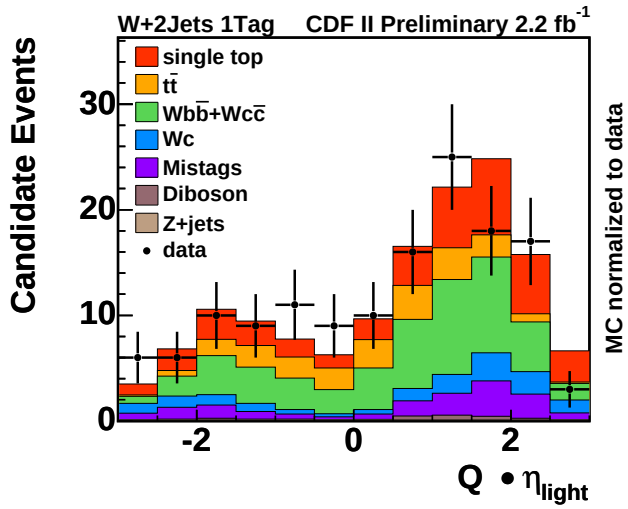

(e)$Q \cdot \eta_{light}$, $NN > 0.4$

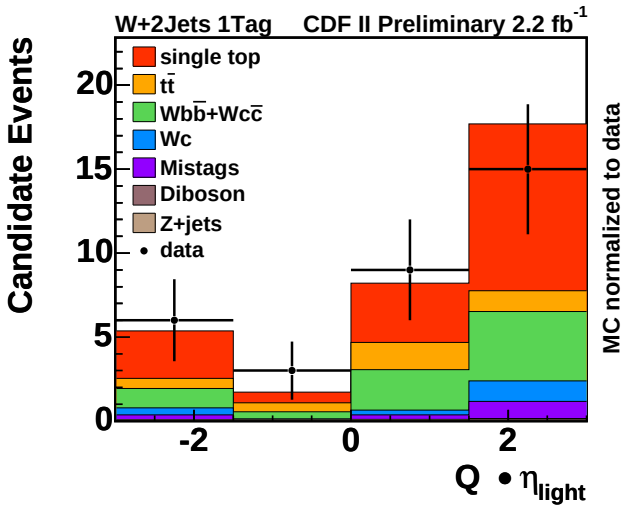

(f)$Q \cdot \eta_{light}$, $NN > 0.8$

FIG. 10: High NN output region. Shown are the reconstructed top mass, the output of the KIT flavor separator, and the product of the lepton-charge and the pseudo-rapidity of the light-quark jet. Left: $NN > 0.4$, right: $NN > 0.8$.

IX. CONCLUSIONS

We present a search of single top–quark production in a CDF II data set corresponding to 2.2 pb^{-1}, assuming a top quark mass of 175 GeV/c^2. We employ neural networks to construct a discriminant between single top–quark events and background events. In a combined search, where t- and s-channel single-top events are regarded as signal, we find an expected p-value of 0.0000053 which corresponds to a sensitivity of 4.4 σ. In data we see evidence for single top. and compute a p-value of 0.00063, corresponding to an observed significance of 3.2 σ.We measure $\sigma_{\mathrm{single\ top}} = 2.0^{+0.9}_{-0.8}$.

[1] D. Acosta *et al.* (CDF Collaboration), *Phys. Rev.* **D65**, 091102 (2002); D. Acosta *et al.* (CDF Collaboration), *Phys. Rev.* **D69**, 052003 (2004); D. Acosta *et al.* (CDF Collaboration), *Phys. Rev.* **D71**, 012005 (2005).

[2] B. Abbott *et al.* (DØ Collaboration), *Phys. Rev.* **D63**, 031101 (2001); V. M. Abazov *et al.* (DØ Collaboration), *Phys. Lett.* **B517**, 282 (2001); V. M. Abazov *et al.* (DØ Collaboration), *Phys. Lett.* **B622**, 265 (2005).

[3] V. M. Abazov *et al.* (DØ Collaboration), *Phys. Rev. Lett.* **98**, 181802 (2007).

[4] B. W. Harris *et al.*, *Phys. Rev.* **D66**, 054024 (2002); Z. Sullivan, *Phys. Rev.* **D70**, 114012 (2004). J. Campbell, R.K. Ellis, F. Tramontano, *Phys. Rev.* **D70**, 094012 (2004).

[5] D. Acosta *et al.* (CDF Collaboration), *Phys. Rev.* **D71**, 052003.